Inorg. Chem. **2006**, *45*, 2509–2519

Photophysics of Platinum–Acetylide Substituted Hexa-*peri*-hexabenzocoronenes

Kye-Young Kim, Shengxia Liu, Muhammet E. Köse, and Kirk S. Schanze*

Department of Chemistry, University of Florida, P.O. Box 117200, Gainesville, Florida 32611-7200

Received October 16, 2005

This manuscript reports the synthesis and photophysical investigation of two hexa-*peri*-hexabenzocoronenes (HBCs) that are functionalized with platinum(II) acetylide units of the type *trans*-(Ar–C≡C–)$_2$Pt(PBu$_3$)$_2$. In one complex, the platinum is directly linked to the HBC chromophore by an ethynyl spacer, whereas in the second, the platinum is separated from the HBC via a 1,4-phenylene ethynylene spacer. The Pt–acetylide units introduce strong spin–orbit coupling into the HBC chromophore, giving rise to high yields of the triplet excited state along with moderately intense phosphorescence at ambient temperature. On the basis of emission spectroscopy, the triplet state of the HBC chromophore is located at 2.14 eV and the S–T splitting is 0.6 eV. The triplet–triplet absorption and radical cation absorption spectra of the Pt–HBCs are determined by laser flash photolysis. Aggregation of the Pt–HBCs in a poor solvent such as hexane leads to quenching of the triplet state, but spectroscopy provides no evidence for the formation of a triplet excimer, even under conditions where the molecules are strongly aggregated.

Introduction

Large polycyclic aromatic hydrocarbons have been the focus of considerable research interest during the past several years. When substituted with alkyl or alkyloxy groups, the structures are soluble in typical organic solvents, and due to the planar, disk shape of the aromatic core the molecules have a strong tendency to aggregate.[1,2] Of particular recent interest is the family of substituted hexa-*peri*-hexabenzocoronenes (HBCs), which have been studied intensively by Müllen and co-workers.[3,4] Although there are early reports concerning the properties of the unsubstituted parent HBC,[5,6] work in this field has been fueled by the development of synthetic approaches that allow relatively large-scale synthesis of a variety of functionalized HBC derivatives.[3,7]

HBCs that are substituted on the periphery with solubilizing alkyl groups aggregate into discotic liquid crystalline phases due to their disk shape and large-area planar π systems.[7−9] A number of investigations have been carried out to characterize the properties of all-organic HBC-based materials.[10,11] These studies have demonstrated that in the solid state the materials display very high charge carrier mobility, an effect which is believed to be due to strong $\pi-\pi$ interactions between adjacent molecules in columnar stacks.[12] Several investigations have also demonstrated that the absorption and fluorescence properties of the HBC chromophore are influenced by aggregation, and the effects are attributed to interchromophore interactions, e.g., π-stacking and singlet excimer formation in the excited state.[9]

Introduction of a transition metal that is strongly coupled to the HBC can provide a means to tune the optical and electronic properties of the chromophore without sacrificing its propensity to self-assemble into aggregates and liquid

* To whom correspondence should be addressed. Tel: 352-392-9133. Fax: 352-392-2395. E-mail: kschanze@chem.ufl.edu.

(1) Gallivan, J. P.; Schuster, G. B. *J. Org. Chem.* **1995**, *60*, 2423−2429.
(2) Nuckolls, C.; Katz, T. J.; Castellanos, L. *J. Am. Chem. Soc.* **1996**, *118*, 3767−3768.
(3) Ito, S.; Wehmeier, M.; Brand, J. D.; Kubel, C.; Epsch, R.; Rabe, J. P.; Müllen, K. *Chem.-Eur. J.* **2000**, *6*, 4327−4342.
(4) Simpson, C. D.; Wu, J. S.; Watson, M. D.; Müllen, K. *J. Mater. Chem.* **2004**, *14*, 494−504.
(5) Clar, E.; Ironside, C. T.; Zander, M. *J. Chem. Soc.* **1959**, 142−147.
(6) Clar, E. *Polycyclic Hydrocarbons*; Academic Press: London, New York, 1964; Vol. 2.
(7) Fechtenkotter, A.; Tchebotareva, N.; Watson, M.; Müllen, K. *Tetrahedron* **2001**, *57*, 3769−3783.
(8) Pisula, W.; Kastler, M.; Wasserfallen, D.; Pakula, T.; Müllen, K. *J. Am. Chem. Soc.* **2004**, *126*, 8074−8075.
(9) Kastler, M.; Pisula, W.; Wasserfallen, D.; Pakula, T.; Müllen, K. *J. Am. Chem. Soc.* **2005**, *127*, 4286−4296.
(10) Wu, J. H.; Watson, M. D.; Müllen, K. *Angew. Chem., Int. Ed.* **2003**, *42*, 5329−5333.
(11) Wu, J. S.; Watson, M. D.; Zhang, L.; Wang, Z. H.; Müllen, K. *J. Am. Chem. Soc.* **2004**, *126*, 177−186.
(12) van de Craats, A. M.; Warman, J. M.; Fechtenkotter, A.; Brand, J. D.; Harbison, M. A.; Müllen, K. *Adv. Mater.* **1999**, *11*, 1469−1472.

10.1021/ic051788v CCC: $33.50
Published on Web 02/11/2006

Chart 1

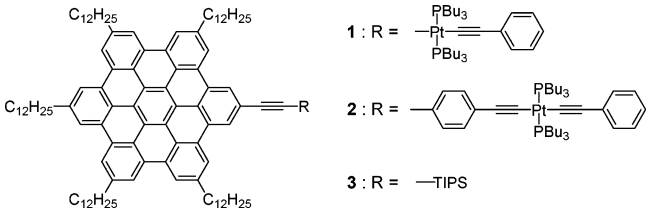

crystalline phases. Although a number of investigations have explored the properties of all-organic HBCs, to date only two metal-organic HBC complexes have been reported.[13,14] This previous investigation examined the optical and electrochemical properties of an N-heterocyclic HBC derivative coordinated to $-Ru(bpy)_2^{2+}$ or $Pd(\eta^3\text{-}C_3H_5)^+$ units.[13,14] The Ru−HBC complex displayed a near-infrared photoluminescence arising from a Ru → HBC metal-to-ligand charge-transfer excited state.

The present manuscript reports the synthesis and photophysical investigation of two HBCs that are functionalized with platinum(II) acetylide units of the type *trans*-$(Ar-C{\equiv}C-)_2Pt(PBu_3)_2$ (structures **1** and **2**, Chart 1). The Pt−acetylide units are of interest because they introduce strong spin−orbit coupling into the HBC chromophore, giving rise to high yields of the triplet excited state along with moderately efficient phosphorescence at ambient temperature.[15−20] The Pt-substituted HBCs are soluble in typical organic solvents, and like the all-organic HBCs, they exhibit a strong tendency to aggregate, even in dilute solution. Because the platinum center enhances intersystem crossing and phosphorescence, it is possible to probe the effect of aggregation of the HBC chromophore on the properties of the triplet excited state in this system. The work presented herein is unique because most previous studies concerning the effects of aggregation on the optical properties of π-conjugated materials have focused on the singlet state.[21−26] This is in part because the singlet state is more easily probed spectroscopically compared to the triplet. The present work provides clear evidence that aggregation of the Pt−HBCs suppresses the triplet yield and lifetime. By contrast, spectroscopic studies show that the electronic structure of the triplet state in the Pt−HBCs is not strongly affected by aggregation, suggesting that triplet state remains localized on a single HBC chromophore despite the existence of intermolecular $\pi-\pi$ interactions in the aggregates.

(13) Draper, S. M.; Gregg, D. J.; Madathil, R. *J. Am. Chem. Soc.* **2002**, *124*, 3486-3487.
(14) Draper, S. M.; Gregg, D. J.; Schofield, E. R.; Browne, W. R.; Duati, M.; Vos, J. G.; Passaniti, P. *J. Am. Chem. Soc.* **2004**, *126*, 8694−8701.
(15) Wilson, J. S.; Köhler, A.; Friend, R. H.; Al-Suti, M. K.; Al-Mandhary, M. R. A.; Khan, M. S.; Raithby, P. R. *J. Chem. Phys.* **2000**, *113*, 7627−7634.
(16) Wilson, J. S.; Chawdhury, N.; Al-Mandhary, M. R. A.; Younus, M.; Khan, M. S.; Raithby, P. R.; Köhler, A.; Friend, R. H. *J. Am. Chem. Soc.* **2001**, *123*, 9412−9417.
(17) Rogers, J. E.; Cooper, T. M.; Fleitz, P. A.; Glass, D. J.; McLean, D. G. *J. Phys. Chem. A* **2002**, *106*, 10108−10115.
(18) Liu, Y.; Jiang, S.; Glusac, K.; Powell, D. H.; Anderson, D. F.; Schanze, K. S. *J. Am. Chem. Soc.* **2002**, *124*, 12412−12413.
(19) Haskins-Glusac, K.; Ghiviriga, I.; Abboud, K. A.; Schanze, K. S. *J. Phys. Chem. B* **2004**, *108*, 4969−4978.
(20) Yam, V. W. W. *Acc. Chem. Res.* **2002**, *35*, 555−563.
(21) Samuel, I. D. W.; Rumbles, G.; Collison, C. J.; Moratti, S. C.; Holmes, A. B. *Chem. Phys.* **1998**, *227*, 75−82.
(22) Yang, J.-S.; Swager, T. M. *J. Am. Chem. Soc.* **1998**, *120*, 11864−11873.
(23) Williams, V. E.; Swager, T. M. *Macromolecules* **2000**, *33*, 4069−4073.
(24) Teetsov, J. A.; Vanden Bout, D. A. *J. Phys. Chem. B* **2000**, *104*, 9378−9387.
(25) Schwartz, B. J. *Annu. Rev. Phys. Chem.* **2003**, *54*, 141−172.
(26) Teetsov, J.; Vanden Bout, D. A. *Langmuir* **2002**, *18*, 897−903.

Experimental Section

General Methods. All starting materials were used without further purification unless otherwise noted. Anhydrous iron(III) chloride (Acros, 98%) was used as received. All reactions were carried out under argon atmosphere with freshly distilled solvents. 4-Dodecylphenylacetylene and compounds **5**, **8**, and **9** were synthesized according to literature procedures.[3,18] Column chromatography was performed on silica gel (Supelco). ^{1}H, ^{13}C, and ^{31}P NMR spectra were recorded on Varian Mercury 300 or Gemini 300 MHz spectrometers; chemical shifts (δ) are reported in ppm and referenced to TMS or protiated solvent signals. ^{31}P NMR chemical shifts were referenced to 80% H_3PO_4. Mass spectra were recorded on Finnigan MAT95Q Hybrid Sector (EI, HRMS) or Bruker Reflex II (MALDI-TOF) mass spectrometers. ^{1}H NMR spectra of **1**, **2**, **3**, **6**, and **7** and ^{31}P NMR spectra of **1** and **2** are provided in the Supporting Information.

4-Iodo-4′-dodecyldiphenylacetylene (4). A degassed solution of 4-dodecyl-phenylacetylene[3] (1.50 g, 5.55 mmol) in THF (10 mL) was added dropwise via a cannula to a degassed solution of *p*-diiodobenzene (5.49 g, 16.6 mmol), $PdCl_2(PPh_3)_2$ (12 mg, 17 μmol), CuI (3 mg), and diisopropylamine (10 mL) in THF (20 mL). The mixture was stirred at room temperature for 5 h. The mixture was passed through a pad of Celite, and the solvent was removed in vacuo. The resulting residue was purified by column chromatography on silica gel. Elution with hexane gave **4** as a white solid (1.3 g, 50%): ^{1}H NMR (300 MHz, $CDCl_3$) δ 7.68 (d, J = 8.5 Hz, 2H), 7.43 (d, J = 8.5 Hz, 2H), 7.24 (d, J = 8.5 Hz, 2H), 7.16 (d, J = 8.5 Hz, 2H), 2.61 (t, J = 7.5 Hz, 2H), 1.60 (t, J = 6.9 Hz, 2H), 1.31−1.25 (m, 18H), 0.88 (t, J = 6.7 Hz, 3H). ^{13}C NMR (76 MHz, $CDCl_3$) δ 143.75, 137.42, 133.01, 131.46, 128.49, 122.99, 119.92, 93.81, 91.02, 87.78, 35.93, 31.93, 31.25, 29.68, 29.65, 29.59, 29.49, 29.37, 29.25, 22.71, 14.16. EI/HRMS calcd: 472.1627; found: 472.1615.

4-Iodo-4′,4″,4‴,4⁗,4⁗′-pentadodecylhexaphenylbenzene (6). Compound **4** (134 mg, 0.284 mmol), **5** (300 mg, 0.284 mmol), and diphenyl ether (2 mL) were placed in a Teflon-top sealed pressure tube, and the reaction mixture was heated at reflux for 7 h in a sand bath. During the reflux period, the temperature of the reaction vessel was carefully maintained at 260 °C. After cooling, the reaction mixture was added dropwise to ethanol (100 mL) with vigorous stirring. After this solution was kept in the refrigerator overnight, the solvent was decanted to give a yellow-brown oil. The oil was purified by column chromatography on silica gel with hexane/CH_2Cl_2 (10:1) to afford **6** as a waxy solid (277 mg, 65%). ^{1}H NMR (300 MHz, $CDCl_3$) δ 7.14 (d, J = 8.4 Hz, 2H), 6.65−6.61 (m, 20H), 6.54 (d, J = 8.4 Hz, 2H), 2.38−2.30 (m, 10H), 1.45−1.10 (m, 100H), 0.88 (t, J = 6.8 Hz, 15H). EI/HRMS calcd: 1502.0782; found: 1502.0784.

2-Iodo-5,8,11,14,17-pentadodecylhexa-*peri*-hexabenzocoronene (7). Compound **6** (250 mg, 0.168 mmol) was dissolved in CH_2Cl_2 (120 mL), and a stream of argon was bubbled through the solution. Iron(III) chloride (0.54 g, 3.3 mmol) was dissolved in nitromethane (7 mL) and added dropwise to the solution of **6**. The mixture was stirred at room temperature for 2 h, and the resulting

green solution was added dropwise to MeOH (150 mL) with stirring. The resulting yellow precipitate was collected by suction filtration using a sintered glass filter and washed with MeOH followed by hexane. The residue was redissolved in small amount of CH_2Cl_2, and the above workup procedure was repeated twice to afford **7** as an off-yellow powder. (175 mg, 70%). ^{1}H NMR (300 MHz, $CDCl_3$) δ 8.10 (br s, 2H), 8.04 (br s, 2H), 7.97 (br s, 2H), 7.74 (br s, 2H), 7.65 (br s, 2H), 7.50 (br s, 2H), 3.02 (br t, 2H), 2.83 (br t, 4H), 2.62 (br t, 4H), 2.08 (br, 2H), 1.93 (br, 4H), 1.80 (br, 4H), 1.65−1.2 (m, 90H), 0.90 (t, J = 7.6 Hz, 15H). MS (LDL-TOF) calcd: 1490.1; found: 1490.8.

2-Triisopropylsilylethynyl-5,8,11,14,17-pentadodecylhexa-*peri*-hexabenzocoronene (3). Compound **7** (170 mg, 0.114 mmol), triisopropylsilylacetylene (31 mg, 0.17 mmol), $Pd(PPh_3)_4$ (6.6 mg, 5.7 μmol), and CuI (2 mg) in piperidine/THF (1 mL/2 mL) were stirred at 40 °C for 4 h. The solvent was evaporated, the residue was redissolved in a minimal amount of CH_2Cl_2, and the solution was added dropwise to MeOH. The resulting precipitate was collected by suction filtration on a fritted glass filter and purified by column chromatography on silica gel with hexane/CH_2Cl_2 2:1 to afford **3** as a yellow solid (137 mg, 78%). ^{1}H NMR (300 MHz, $CDCl_3$) δ 8.29 (br s, 2H), 7.98 (br s, 2H), 7.88 (br s, 6H), 7.85 (br s, 2H), 3.00 (br t, J = 7.8 Hz, 4H), 2.90 (br t, J = 6.3 Hz, 6H), 2.00 (br m, 10H), 1.67−1.25 (m, 108H), 0.87−0.83 (m, 15H). MS (LDL-TOF) calcd: 1544.6; found: 1544.4.

Complex 1. A stirred solution of **3** (100 mg, 48 μmol), **8** (38 mg, 52 μmol), $Pd(PPh_3)_4$ (5.6 mg, 4.8 μmol), and CuI (2 mg) in piperidine/THF (2 mL, 1:1 v/v) was degassed with argon for 20 min. Tetrabutylammonium fluoride (1 M in THF, 100 μL) was added to the reaction mixture via a microsyringe. The mixture was stirred at 40 °C. After 5 h, the solvent was removed under a stream of argon. The residue was redissolved in a small amount of CH_2Cl_2, and the resulting solution was added dropwise to MeOH (100 mL) with stirring. The precipitate was collected by suction filtration and purified by column chromatography on silica gel (petroleum ether/CH_2Cl_2, 2:1−1:3) to give **1** (68 mg, 68%). A second purification by preparative thin-layer chromatography on silica gel (hexane/CH_2Cl_2 3:2) yielded **1** as a yellow solid (45 mg, 45%). ^{1}H NMR (300 MHz, CD_2Cl_2) δ 8.99 (br s, 2H), 8.75 (br s, 2H), 8.49 (br s, 2H), 8.23 (br s, 2H), 7.90 (br s, 2H), 7.76 (br s, 2H), 7.37 (d, J = 7.2 Hz, 2H), 7.28 (t, J = 7.2 Hz, 2H), 7.18 (t, J = 7.3 Hz, 1H), 3.24 (t, J = 7.4 Hz, 4H), 2.88 (t, J = 7.2 Hz, 4H), 2.68 (t, J = 7.2 Hz, 2H), 2.44 (m, 12H), 2.11 (m, 4H), 1.92−1.20 (m, 110 H), 1.14 (t, J = 7.2 Hz, 18H), 0.87−0.83 (m, 15H). ^{31}P NMR (121 MHz, CD_2Cl_2) δ 4.77 (J_{Pt-P} = 2354 Hz). MS (LDL-TOF): calcd: 2088.0; found: 2088.0.

Complex 2. A solution of **7** (80 mg, 54 μmol), **9** (49 mg, 59 μmol), $Pd(PPh_3)_4$ (6.2 mg, 5.4 μmol), and CuI (2 mg) in piperidine/THF (2 mL, 1:1 v/v) was stirred and degassed for 20 min with argon. The reaction mixture was then stirred while heating to 40 °C for 5 h. After cooling, the solvent was evaporated under a stream of argon. The residue was redissolved in a small volume of CH_2Cl_2, and the resulting solution was added dropwise into MeOH (100 mL) with stirring. The precipitate was collected by suction filtration and purified by column chromatography on silica gel (petroleum ether/CH_2Cl_2, 3:1−1:3) to give **2** as a yellow solid (89 mg, 75%). A second column chromatography of **2** on silica gel (hexane/CH_2Cl_2, 3:2) yielded pure **2** as a yellow solid (63 mg, 53%). ^{1}H NMR (300 MHz, CD_2Cl_2) δ 8.30 (br s, 2H), 8.16 (br s, 2H), 8.04 (br s, 4H), 8.01 (br s, 2H), 7.99 (br s, 2H), 7.78 (d, J = 8.0 Hz, 2H), 7.50 (d, J = 8.0 Hz, 2H), 7.31 (d, J = 6.9 Hz, 2H), 7.25 (t, J = 7.4 Hz, 2H), 7.15 (t, J = 7.2 Hz, 1H), 2.91 (br m, 10H), 2.25 (m, 12H), 1.98 (br m, 10H), 1.91−1.23 (m, 104 H), 1.07 (t, J = 7.2 Hz, 18H), 0.89 (m, 15H). ^{31}P NMR (121 MHz, $CDCl_3$) δ 4.59 (J_{Pt-P} = 2346 Hz). MS (LDL-TOF): calcd: 2188.2; found: 2188.5.

Photophysical Measurements. All photophysical studies were carried out with solutions contained in 1 × 1 cm^2 quartz cells and degassed by using argon bubbling unless otherwise noted. For emission measurements, sample concentrations were adjusted to produce optically dilute solutions (A_{max} < 0.1, $c \approx 5 \times 10^{-7}$ M). Transient absorption measurements were carried out with solutions having A = 0.8−1.0 at 355 nm. UV−visible absorption spectra were recorded on a Varian Cary 100 dual-beam spectrophotometer. Corrected steady-state emission measurements were performed on a SPEX Fluorolog 3 fluorescence spectrometer. Emission quantum yields were measured by relative actinometry with 9,10-dicyanoanthracene in argon-degassed EtOH (Φ_{em} = 0.89) as an actinometer.[27] Fluorescence decays were obtained by time-correlated single photon counting on an instrument that was constructed in-house. Excitation was effected by using a violet diode laser (405 nm, IBH instruments, Edinburgh, Scotland, pulse width 800 ps). The time-resolved emission was collected using a red-sensitive, photon-counting PMT (Hamamatsu R928), and the light was filtered using 10 nm bandpass interference filters. Lifetimes were determined from the observed decays with the DAS6 deconvolution software (IBH instruments, Edinburgh, Scotland). The goodness of the fits was evaluated by χ^2 values <1.3 and by inspection of the residual plots. Phosphorescence decays were measured on an apparatus consisting of a Continuum Surelite II Nd:YAG laser as a source (third harmonic, λ = 355 nm, 10 ns fwhm) with time-resolved detection provided by an intensified CCD detector (Princeton Instruments, PI-MAX iCCD) coupled to an Acton SpectraPro 150 spectrograph. Transient absorption spectra were obtained on an instrument that has been previously described that uses the third harmonic of a Nd:YAG laser (Spectra Physics GCR-14, 355 nm, 10 ns fwhm, 10 mJ pulse^{-1}, 20 mJ cm^{-2} irradiance) as excitation source.[28]

Electrochemical Measurements. Electrochemical studies employed cyclic voltammetry using a BAS CV-50W voltammetric analyzer. The three-electrode system was equipped with a glassy carbon disk (1.6 mm diameter) working electrode, a silver wire reference electrode, and a Pt wire counter electrode. The electrochemical potentials were calibrated relative to the saturated calomel electrode (SCE) by using ferrocene as an internal standard (Fc/Fc^+ at +0.40 V vs SCE). Tetra-*n*-butylammonium hexafluorophosphate (0.1 M) in CH_2Cl_2 was used as supporting electrolyte.

Density Functional Calculations. Quantum chemical calculations were carried out by using the Gaussian 03 program.[29] For the parent structure, HBC, the B3LYP hybrid functional was used along with the 6−31g* basis set. The molecule has D_{6h} symmetry, and

(27) Murov, S. L.; Carmichael, I.; Hug, G. L. *Handbook of Photochemistry*, 2nd ed.; Marcel Dekker: New York, 1993.
(28) Wang, Y. S.; Schanze, K. S. *Chem. Phys.* **1993**, *176*, 305−319.
(29) Frisch, M. J.; Trucks, G. W.; Schlegel, H. B.; Scuseria, G. E.; Robb, M. A.; Cheeseman, J. R.; Montgomery, J. A., Jr.; Vreven, T.; Kudin, K. N.; Burant, J. C.; Millam, J. M.; Iyengar, S. S.; Tomasi, J.; Barone, V.; Mennucci, B.; Cossi, M.; Scalmani, G.; Rega, N.; Petersson, G. A.; Nakatsuji, H.; Hada, M.; Ehara, M.; Toyota, K.; Fukuda, R.; Hasegawa, J.; Ishida, M.; Nakajima, T.; Honda, Y.; Kitao, O.; Nakai, H.; Klene, M.; Li, X.; Knox, J. E.; Hratchian, H. P.; Cross, J. B.; Bakken, V.; Adamo, C.; Jaramillo, J.; Gomperts, R.; Stratmann, R. E.; Yazyev, O.; Austin, A. J.; Cammi, R.; Pomelli, C.; Ochterski, J. W.; Ayala, P. Y.; Morokuma, K.; Voth, G. A.; Salvador, P.; Dannenberg, J. J.; Zakrzewski, V. G.; Dapprich, S.; Daniels, A. D.; Strain, M. C.; Farkas, O.; Malick, D. K.; Rabuck, A. D.; Raghavachari, K.; Foresman, J. B.; Ortiz, J. V.; Cui, Q.; Baboul, A. G.; Clifford, S.; Cioslowski, J.; Stefanov, B. B.; Liu, G.; Liashenko, A.; Piskorz, P.; Komaromi, I.; Martin, R. L.; Fox, D. J.; Keith, T.; Al-Laham, M. A.; Peng, C. Y.; Nanayakkara, A.; Challacombe, M.; Gill, P. M. W.; Johnson, B.; Chen, W.; Wong, M. W.; Gonzalez, C.; Pople, J. A. *Gaussian 03*; Gaussian, Inc.: Wallingford, CT, 2004.

Scheme 1 [a]

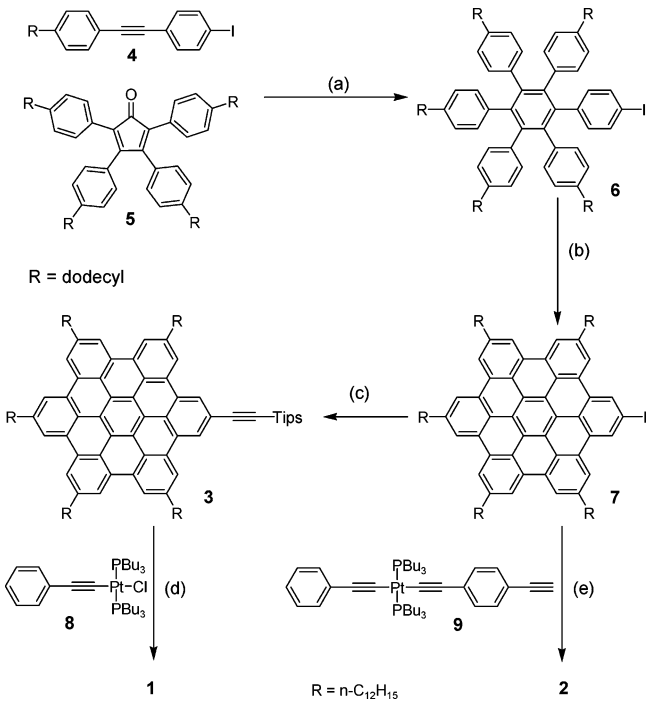

[a] (a) Ph_2O, reflux, 65%; (b) $FeCl_3$, CH_3NO_2/CH_2Cl_2, 70%; (c) triisopropylsilylacetylene, $Pd(PPh_3)_4$, CuI, piperidine, 40 °C, 78%; (d) CuI, piperidine, $^nBu_4NF$, 40 °C, 45%; (e) $Pd(PPh_3)_4$, CuI, piperidine, 40 °C, 53%.

the calculations were carried out within this symmetry. Structure **3** was optimized under C_{2v} symmetry restriction by using the same functional and basis set used for HBC. Calculations on Pt−HBC **1** were carried out by using the B3LYP hybrid; however, for this system, the SDD basis set was used to employ Stuttgart/Dresden relativistic effective core potential for explicit treatment of platinum electrons, and the geometry was optimized within C_s symmetry. The alkyl chains in **1** and **3** were truncated to either hydrogen or methyl groups to save computational time in calculations. All time-dependent density functional theory (TD-DFT) calculations were performed with the same basis sets and methods used for geometry optimizations for the corresponding structure.

Results and Discussion

Structure and Synthesis. Chart 1 shows the structures of the three HBCs prepared in this study. Each of the HBCs is functionalized with five linear C_{12} chains to facilitate solubility. Complexes **1** and **2** contain the HBC unit coupled to a *trans*-$Pt(PBu_3)_2(C{\equiv}C-Ar)_2$ chromophore. In complex **1**, the HBC chromophore is coupled to the Pt center via a single ethynyl linker, whereas in complex **2**, the HBC chromophore is separated from the Pt center by a 1,4-phenylene ethynylene "spacer". The effect of the phenylene ethynylene spacer on the optical and aggregation properties of the complexes will be evident below. HBC **3** is a synthetic precursor for **1** and **2** and was selected as a model to provide information on the photophysics of the ethynyl-substituted HBC chromophore.

The overall synthetic route used to obtain the HBC derivatives is illustrated in Scheme 1. The key intermediate is the iodo-substituted HBC **7**, which is a new compound. This material was synthesized by a method analogous to that used by Müllen and co-workers to prepare the corresponding monobrominated HBC derivative.[3] Thus, the Diels−Alder reaction of alkyl-substituted tetracyclone **5** with 4-iodo-4′-dodecyldiphenylacetylene (**4**) in diphenyl ether affords hexaphenylbenzene derivative **6** in 30−70% yield, and subsequent oxidative dehydrogenation of **6** with iron(III) chloride provides **7** in good yield. Although Diels−Alder reactions of tetracyclones with diarylacetylenes to afford polyphenyl-substituted aromatic hydrocarbons have been reported many times,[3,30−32] in our hands, it was observed that the yield of **6** was highly variable. Careful study of this reaction showed that the yield varied strongly with temperature. It was found that the yield was optimum when the reaction was carried out with the vessel maintained at 260 °C, a temperature at which the diphenyl ether solvent is gently refluxing. If the reaction is run at slightly lower temperatures (e.g., 200−240 °C), the Diels−Alder reaction is slow, and **5** undergoes a competitive thermal decomposition reaction which reduces the yield of the desired product. To accomplish the construction of Pt−acetylide HBCs, the iodo-substituted HBC **7** was functionalized with TIPS−acetylene to give **3**. In-situ deprotection of the TIPS group followed by Hagihara coupling with platinum(II) chloride complex **8** afforded Pt−HBC **1**. Sonogashira coupling of iodo-HBC **7** with **9** afforded **2**.

In contrast to other reported HBC derivatives, **1** and **2** are soluble in most organic solvents, likely due to the symmetry breaking effect of the Pt-substitution on the HBC, along with the effect of the tributylphosphine ligands on the Pt center. The good solubility characteristics of the compounds facilitated their purification by column chromatography and allowed photophysical measurements to be carried out in a variety of solvents. The structures of **1**−**3** were characterized by ^1H and ^{31}P NMR spectroscopy and MALDI-TOF mass spectrometry (the NMR spectra are included as Supporting Information). The ^1H NMR spectra of **1** and **2** in CD_2Cl_2 feature well-resolved, yet slightly broadened resonances in the aromatic region compared to the aromatic resonance signals from **6**, indicating that the complexes aggregate as previously reported for other HBC derivatives.[9]

More information concerning aggregation of **2** comes from a study of the effect of concentration on its ^1H NMR spectrum (see Figure S-8 in the Supporting Information). In particular, for a 0.01 M solution of complex **2** in CD_2Cl_2, the resonance signals for the aromatic HBC protons appear at $\delta \approx 7.8-8.2$ ppm. As the solution is diluted, the aromatic HBC protons shift downfield. In a 3×10^{-5} M solution, the five sets of HBC aromatic protons in **2** appear in the range from 8.4 to 8.9 ppm. The α- and β-methylene groups on the HBC-tethered alkyl chains also shift downfield with decreasing concentration. For example, the α-CH_2 signals shift from 2.65 to 3.15 ppm as the sample is diluted from 0.01 to 3×10^{-5} M. The solvent dependence of the NMR spectrum of **2**

(30) Sadhukhan, S. K.; Viala, C.; Gourdon, A. *Synthesis (Stuttgart)* **2003**, 1521−1525.
(31) Harvey, J. A.; Ogliaruso, M. A. *J. Chem. Eng. Data* **1977**, *22*, 110−113.
(32) Samanta, S. R.; Mukherjee, A. K.; Bhattacharya, A. J. *Indian J. Chem., Sect. B: Org. Chem. Incl. Med. Chem.* **1985**, *24*, 960−961.

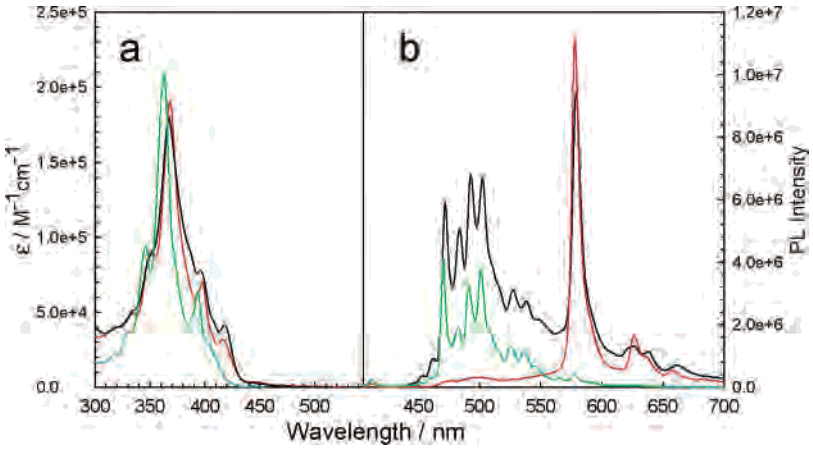

Figure 1. (a) Absorption and (b) photoluminescence spectra of **1** (red), **2** (black), and **3** (green) in THF solution. Photoluminescence spectra were obtained in argon-deoxygenated solution, $c = 5 \times 10^{-7}$ M.

is consistent with observations on a series of symmetrical hexa-alkyl-chain substituted-HBCs, in which it was shown that the signals for the aromatic HBC protons shift downfield with decreasing concentration.[9] The upfield shift at higher concentration is attributed to aggregation of the HBC in solution.

Absorption and Photoluminescence Spectroscopy: the Singlet and Triplet Excited States in the HBC Chromophore. The absorption and photoluminescence spectra of **1**−**3** were examined in a variety of solvents in very dilute solutions ($c \approx 5 \times 10^{-7}$ M), and in this study, it was found that aggregation is minimized in THF (vide infra). Thus, studies carried out in this solvent provide the best available information concerning the photophysics of the Pt−HBCs in a nonaggregated state. Figure 1a illustrates the absorption spectra of **1**−**3** in THF solution. First, the absorption of TIPS−HBC **3** is similar to that of other all-organic HBCs;[5,6,33,34] the spectrum features a weak onset at ca. 425 nm, with band maxima at 393, 363, and 346 nm. Interestingly, the 363 nm band is the most intense, whereas the 393 nm band and the low-energy tail are considerably less intense. In view of the fact that, in analogy to benzene, the HBC chromophore has D_{6h} symmetry, it is likely that the unusual shape of the absorption spectrum derives from the fact that the lowest-energy tail arises from one or more symmetry-forbidden transitions, whereas the intense 363 nm absorption is due to a symmetry-allowed transition.[35,36] This hypothesis is supported by density functional calculations presented below.

The absorption spectra of Pt−HBCs **1** and **2** are very similar to that of **3** with a few key differences. First, the dominant HBC-based bands seen in **3** appear in the spectra of **1** and **2** with slight red-shifts. More importantly, both of the Pt−HBCs exhibit an additional, moderately intense absorption band with $\lambda_{max} \approx 416$ nm ($\epsilon \approx 3-4 \times 10^4$ M^{-1} cm^{-1}). This band is believed to arise due to the presence of the Pt−acetylide unit, which breaks the symmetry of the HBC chromophore and extends the π conjugation along the Pt−acetylide axis. This assignment is also supported by the calculations that are presented below. A subtle, yet noteworthy, point is that the absorption bands in the spectrum of **2** are less well resolved compared to those of **1**. This feature suggests that **2** has a larger self-association constant than that of **1**, and therefore is aggregated to some extent even in THF solution with $c = 0.5$ μM.

The photoluminescence spectra of **1**−**3** in argon degassed solutions are shown in Figure 1b, and emission lifetimes and quantum yields (τ_{em} and ϕ_{em}, respectively) are listed in Table 1. TIPS−HBC **3** exhibits a moderately intense fluorescence that appears as a broad band with a complex vibronic structure. The fluorescence is similar to that of symmetric hexa-alkyl-substituted HBCs, which indicates that the ethynyl substituent has little effect on the fluorescence.[9,33,34,37] There are several significant features with respect to the fluorescence of **3**. First, the intensity at the emission's origin is low ($\lambda \approx 452$ nm), and there is an apparent Stokes shift between the fluorescence and absorption onsets. This strongly suggests that the transition from the lowest singlet excited state to the ground state is forbidden. This notion is supported by the observation that the fluorescence lifetime is relatively long ($\tau \approx 45$ ns). This finding is consistent with the premise suggested above that the lowest singlet excited state in the HBC chromophore is symmetry forbidden.[34−36] In addition, the complexity of the overall fluorescence spectrum strongly suggests that there are several singlet excited states that are in close energetic proximity which contribute to the fluorescence, each having its own vibronic progression.

The striking feature in the photoluminescence of Pt−HBCs **1** and **2** is the additional, narrow-bandwidth emission with $\lambda_{max} \approx 578$ nm. This band is clearly due to phosphorescence from the HBC chromophore,[38] and the phosphorescence assignment is supported by the emission lifetime which is greater than 20 μs for both complexes (Table 1). The phosphorescence is observed in the Pt−HBCs because spin−

(33) Wang, Z. H.; Tomovic, E.; Kastler, M.; Pretsch, R.; Negri, F.; Enkelmann, V.; Müllen, K. *J. Am. Chem. Soc.* **2004**, *126*, 7794−7795.
(34) Biasutti, M. A.; Rommens, J.; Vaes, A.; De Feyter, S.; De Schryver, F. D.; Herwig, P.; Müllen, K. *Bull. Soc. Chim. Belg.* **1997**, *106*, 659−664.
(35) Klevens, H. B.; Platt, J. R. *J. Chem. Phys.* **1949**, *17*, 470−481.
(36) Platt, J. R. *J. Chem. Phys.* **1949**, *17*, 484−495.
(37) Wu, J. S.; Watson, M. D.; Tchebotareva, N.; Wang, Z. H.; Müllen, K. *J. Org. Chem.* **2004**, *69*, 8194−8204.

Table 1. Photophysical Data for **1**−**3**[a]

	PL (λ_{max}/nm)		Φ_{em}[b,c]		τ_F/ns[d]	τ_p/ns[e]	τ_p(TA)/μs[f]		
	F	P	THF	CH_2Cl_2	THF	THF	THF	CH_2Cl_2	hexane
1	472	578	0.13 $\Phi_F = 0.0096$ $\Phi_P = 0.12$	0.028	32 (64%) 3.0 (36%)	215	130	22	12
2	472	579	0.17 $\Phi_F = 0.11$ $\Phi_P = 0.058$	0.079	47 (95%) 9.8 (5%)	33	40	20	8
3	470	−	0.12	0.097	45 (86%) 8.6 (14%)	−	−	−	−

[a] All measurements were conducted on argon-degassed THF solutions at 298 K unless otherwise noted. [b] Photoluminescence quantum yields are relative to 9,10-dicyanoanthracene in ethanol solution, $\Phi_{em} = 0.89$. [c] Measurements were taken on solutions with matched optical density at 377 nm, $c \approx 2 \times 10^{-7}$ M. [d] Fluorescence lifetimes. Decays were biexponential; numbers in parentheses indicated relative amplitude of component. [e] Phosphorescence decay lifetimes. [f] Transient absorption decay lifetimes.

orbit coupling from the metal center increases the rates of $S_1 \rightarrow T_1$ intersystem crossing and $T_1 \rightarrow S_o$ radiative decay. Interestingly, in complex **1**, where the Pt complex is separated from the HBC chromophore by an ethynyl group, very little fluorescence is observed ($\phi_f \approx 0.01$), suggesting that $S_1 \rightarrow T_1$ intersystem crossing is very rapid. By contrast, in **2** where the Pt complex is separated from the HBC chromophore by a phenyl-ethynyl spacer, the fluorescence is considerably stronger ($\phi_f \approx 0.11$), signaling that in this system $S_1 \rightarrow T_1$ intersystem crossing is less competitive with radiative decay of the singlet state. Despite these differences, the phosphorescence energy and band shape are almost identical in **1** and **2**, which indicates that the lowest triplet is localized on the HBC chromophore. In both complexes, the phosphorescence is dominated by the 0−0 band, with a weak, but discernible vibronic progression observed with 0−1, 0−2, and 0−3 bands at 1327, 1602, and 2126 cm^{-1}, respectively. The first two bands are likely C−C stretching modes of the HBC aromatic ring system, whereas the 0−3 band is likely due to the C≡C stretch. The fact that the phosphorescence 0−0 band is considerably more intense compared to the vibronic overtones indicates that the geometry of the triplet state is very similar to that of the ground state, consistent with the rigid structure of the HBC ring system. The emission of **2** was also examined at 80 K in a rigid 2-methyltetrahydrofuran (2-MTHF) solvent glass (see Figure S-2 in the Supporting Information). Although the emission energy and band shape at 80 K are very similar to those observed at ambient temperature, one subtle effect was noticed. In particular, the 0−0 phosphorescence band has two shoulders that are shifted to slightly longer wavelength. Similar splitting in the phosphorescence has been observed in other platinum−acetylide systems at low temperature, and in those systems, it has been attributed to the existence of different conformers that cannot equilibrate in the frozen matrix.[39] A similar effect may be operating in complex **2** because in the frozen 2-MTHF glass rotation around the C≡C bonds is not possible.

The observation of HBC-based phosphorescence from **1** and **2** allows us to assign the triplet energy of the HBC chromophore as ca. 2.14 eV (49.4 kcal mol^{-1}). Taking the lowest singlet excited-state energy from the onset of the fluorescence for **2** ($\lambda \approx 454$ nm, 2.73 eV) allows derivation of the singlet−triplet splitting for the HBC chromophore ($\Delta E_{ST} = E_s - E_T \approx 0.6$ eV). This value is remarkably small by comparison with values for other condensed polycyclic aromatic hydrocarbons, which range from 1.5 eV for naphthalene to 0.9 eV for chrysene.[27,40] The small ΔE_{ST} for the HBC chromophore underscores the fact that the singlet excited state is strongly delocalized within the 14-ring system. This is because a significant component of the singlet−triplet splitting arises from electron−electron repulsion in the singlet state, which is decreased by spatial delocalization of the excited-state wave function.[41]

Density Functional Calculations. To provide insight regarding the electronic basis for the lowest excited states of the HBC chromophore, density functional theory (DFT) calculations were carried out on the parent molecule HBC, as well as on derivatives **1** and **3**. The parent HBC chromophore has very high symmetry, and comparison of the results on the parent with those of **3** provide insight concerning the effect of the ethynyl substituent on the electronic structure of the HBC chromophore. The calculations on Pt−HBC complex **1** reveal how the metal interacts with the HBC chromophore. The geometry of each structure was optimized by using DFT, and then time-dependent DFT (TD-DFT) was used to compute the optical transition energies. The results of the calculations for the three compounds are listed in Table 2. Frontier orbital density plots for **1** are shown in Figure 2, whereas those for HBC and **3** are provided as Supporting Information.

Calculations for the parent HBC were carried out in D_{6h} symmetry. Not surprisingly, the results show that there is a direct parallel between the symmetry and structure of the frontier orbitals for the HBC chromophore and benzene, which also has D_{6h} symmetry. In particular, the HOMO and LUMO orbitals of HBC are doubly degenerate (E_{1g} and E_{2u}, respectively, see Supporting Information for orbital plots). Transitions between these levels give rise to three types of

(38) While this is the first unambiguous report of phosphorescence from an HBC, in a hydrocarbon review published in 1962, E. Clar noted that "A weak solution (of hexa-*peri*-benzocoronene) in trichlorobenzene cooled in liquid nitrogen shows a strong orange phosphorescence (band at 5750 Å) of long life after irradiation with a mercury lamp", ref 6.

(39) Haskins-Glusac, K., Ph.D. Dissertation, University of Florida, Gainesville, 2003, http://www.chem.ufl.edu/~kschanze/dissertations.htm.

(40) Turro, N. J. *Modern Molecular Photochemistry*; Benjamin/Cummings: Menlo Park, CA, 1978.

(41) McGlynn, S. P.; Smith, F. J.; Cilento, G. *Photochem. Photobiol.* **1964**, *3*, 269−294.

Table 2. Results of TD-DFT Calculations on HBC, **1**, and **3**

	HBC		**3**		**1**	
state	*a*	*b*	*a*	*b*	*a*	*b*
1	$^1B_{2u}$ 428 nm $f = 0.0000$	H − 1 → L, 50% H → L + 1, 50%	$^1B_2$ 433 nm $f = 0.0001$	H − 1 → L, 51% H → L + 1, 49%	$^1A''$ 441 nm $f = 0.0048$	H − 2 → L + 1 5% H − 1 → L, 39% H → L + 1, 53% H → L + 2, 3%
2	$^1B_{1u}$ 409 nm $f = 0.0000$	H − 1 → L + 1, 50% H → L, 50%	$^1A_1$ 415 nm $f = 0.0167$	H − 1 → L + 1, 41% H → L, 59%	$^1A'$ 423 nm $f = 0.1513$	H − 2 → L, 2% H − 1 → L + 1, 25% H → L, 73%
3	$^1E_{2g}$ 381 nm $f = 0.0000$	H − 2 → L, 20% H → L + 2, 80%	$^1B_2$ 381 nm $f = 0.0028$	H − 2 → L, 23% H → L + 2, 77%	$^1A''$ 404 nm $f = 0.0025$	H − 4 → L, 7% H → L + 1, 7% H → L + 2, 86%
4	$^1E_{2g}$ 377 nm $f = 0.0000$	H − 2 → L + 1, 20% H − 1 → L + 2, 80%	$^1A_1$ 376 nm $f = 0.0119$	H − 2 → L + 1, 20% H − 1 → L + 2, 80%	$^1A'$ 404 nm $f = 0.1238$	H − 4 → L + 1, 11% H − 2 → L, 2% H − 1 → L + 1, 23% H − 1 → L + 2, 57% H → L, 7%
5	$^1E_{1u}$ 377 nm $f = 0.6473$	H − 1 → L, 50% H → L + 1, 50%	$^1A_1$ 361 nm $f = 0.8441$	H − 1 → L + 1, 58% H − 1 → L + 2, 4% H → L, 38%	$^1A''$ 394 nm $f = 0.1949$	H − 5 → L + 1, 6% H − 2 → L + 1, 24% H − 1 → L, 34% H → L + 1, 36%
6	$^1E_{1u}$ 374 nm $f = 0.6562$	H − 1 → L + 1, 50% H → L, 50%	$^1B_2$ 361 nm $f = 0.6724$	H − 1 → L, 47% H → L + 1, 49% H → L + 2, 4%	$^1A'$ 383 nm $f = 0.5409$	H − 5 → L, 3% H − 4 → L + 1, 4% H − 2 → L, 23% H − 1 → L + 1, 27% H − 1 → L + 2, 27% H → L, 16%
triplet	n/a 589 nm		$^3A_1$ 595 nm		$^3A'$ 606 nm	

[a] State assignment, wavelength of optical transition and oscillator strength (*f*). [b] Molecular orbital basis for transitions.

configurations ($E_{1g} \otimes E_{2u} = {}^1B_{2u} + {}^1B_{1u} + {}^1E_{1u}$), in direct analogy to the lowest transitions in benzene. Of these three excited-state configurations, transitions from the ground state ($^1A_{1g}$) to $^1B_{2u}$ and $^1B_{1u}$ are dipole forbidden in D_{6h} symmetry, whereas the transition to the $^1E_{1u}$ state is dipole allowed.[42] Time-dependent DFT was carried out on HBC to calculate the energies and oscillator strengths of the lowest optical transitions, and the results are summarized in the first column of Table 2. The TD-DFT calculations predict the dipole forbidden $^1A_{1g} \rightarrow {}^1B_{2u}$ and $^1A_{1g} \rightarrow {}^1B_{1u}$ transitions (1 and 2, Table 2) to occur at 428 and 409 nm, respectively, while the dipole-allowed transitions occur at 377 and 374 nm (transitions 5 and 6, Table 2).

Calculations on **3** were carried out in C_{2v} symmetry. Despite the lower symmetry, the spatial distribution of the frontier orbitals of **3** correspond quite closely with the HOMO (E_{1g}) and LUMO (E_{2u}) levels of HBC. The HOMO and LUMO orbitals (both of B_1 symmetry) feature contributions from the ethynyl substituent. The results of the TD-DFT calculations are listed in Table 2 to allow comparison between the corresponding transitions in **3** and HBC. Note that there is very good agreement between the calculated transitions and the observed absorption spectrum of **3**. In particular, the low-energy tail on the absorption spectrum of **3** has its onset at ca. 425 nm, and the first clearly resolved, weak band has $\lambda_{max} = 393$ nm. These bands likely correspond to $^1A_1 \rightarrow {}^1B_2$ and $^1A \rightarrow {}^1A_1$ (transitions 1 and 2, Table 2); although these transitions are allowed in C_{2v} symmetry, they correlate with the $^1B_{2u}$ and $^1B_{1u}$ transitions, which are dipole forbidden in the D_{6h} local symmetry of the HBC chromophore. The intense transition observed at 363 nm in **3** likely corresponds to $^1A_1 \rightarrow {}^1A_1$ and $^1A_1 \rightarrow {}^1B_2$ (transitions 5 and 6, Table 2); these transitions correlate with the $^1A_{1g} \rightarrow {}^1E_{1u}$ transitions which are dipole allowed in the D_{6h} local symmetry of the HBC chromophore.

Overall, the calculations provide insight into the absorption and fluorescence properties of **3** and structurally related HBCs. In particular, it is evident that the chromophore features two energetically low-lying excited states that are dipole-forbidden. This explains the relatively large apparent Stokes-shift, and the comparatively long fluorescence lifetime (45 ns for **3**). It is possible that the complex structure of the fluorescence spectrum observed for **3** and other HBCs arises because at ambient temperature both the $^1B_{2u}$ and $^1B_{1u}$ states are populated and undergo radiative decay on a comparable time scale.

Turning to the calculation on Pt−HBC **1**, it is first necessary to consider the energetically preferred orientation of the square planar platinum unit (as defined by the PtP_2C_2 moiety) with respect to the HBC plane. Calculations were carried out to explore the ground-state energy as a function of the dihedral angle (θ), which is defined as the relative angle between the HBC plane and the plane defined by the PtP_2C_2 unit. The calculations indicate that the "twisted" conformation with $\theta = 90°$ is preferred by ca. 0.6 kcal mol^{-1} relative to the conformation where the two units are coplanar ($\theta = 0°$). This finding is consistent with recently published theoretical studies of Pt−acetylides which show that the π system of the arylacetylide ligands interacts most strongly with in-plane (d_{xy}) orbital on Pt.[43,44] The HOMO and LUMO

(42) Cotton, F. A. *Chemical Applications of Group Theory*; John Wiley and Sons: New York, 1963.

(43) Emmert, L. A.; Choi, W.; Marshall, J. A.; Yang, J.; Meyer, L. A.; Brozik, J. A. *J. Phys. Chem. A* **2003**, *107*, 11340−11346.

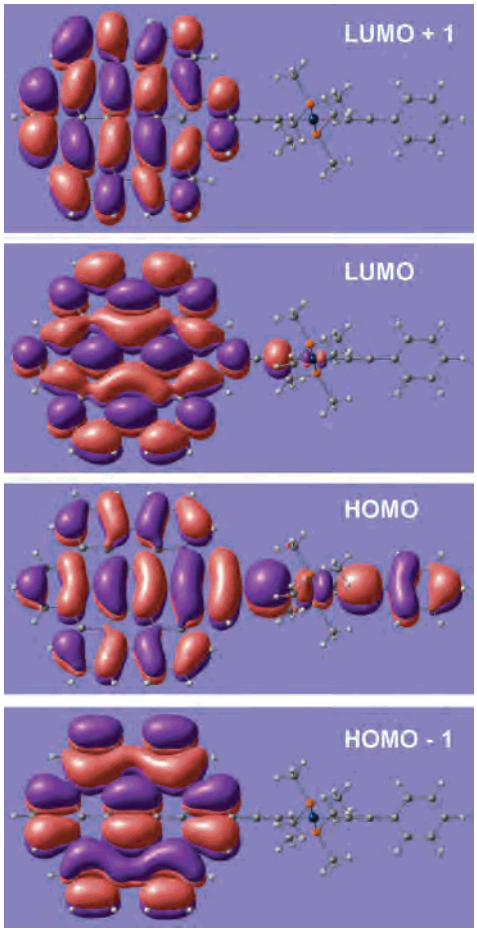

Figure 2. Frontier orbital plots for optimized ground state geometry of Pt−HBC complex **1** computed by using DFT as described in the text.

levels computed for the low-energy "twisted" conformation are shown in Figure 2. The interesting aspect here is that the HOMO is delocalized considerably into the Pt−acetylide substituent. In particular, there is a small contribution to the orbital from the in-plane (d_{xy}) orbital on Pt, and the HOMO is delocalized significantly into the phenylacetylene ligand that is trans to the ethynyl−HBC unit. By contrast, the LUMO is more strongly localized on the HBC core. The results of the TD-DFT calculation on **1** are shown in Table 2. Several features are significant with respect to the results. First, the calculated transitions are shifted to lower energy relative to the position of the corresponding transitions in HBC. This shift arises because the energy of the HOMO in **1** is raised due to interaction with the Pt−acetylide unit. The second point is that there is a significant increase in the oscillator strength of the low-energy transitions; in particular, transition 2, which is dominated by the HOMO → LUMO configuration has $f = 0.15$. The interesting point is that this transition corresponds quite closely to the additional band observed in the absorption spectra of **1** and **2** at $\lambda = 416$ and 418 nm, respectively. Given that the HOMO is delocalized significantly into the Pt−acetylide substituent and the LUMO is largely localized on the HBC core, this low-energy transition is anticipated to have a small degree of charge-transfer character, and it is expected to be polarized along the long axis of the molecule.

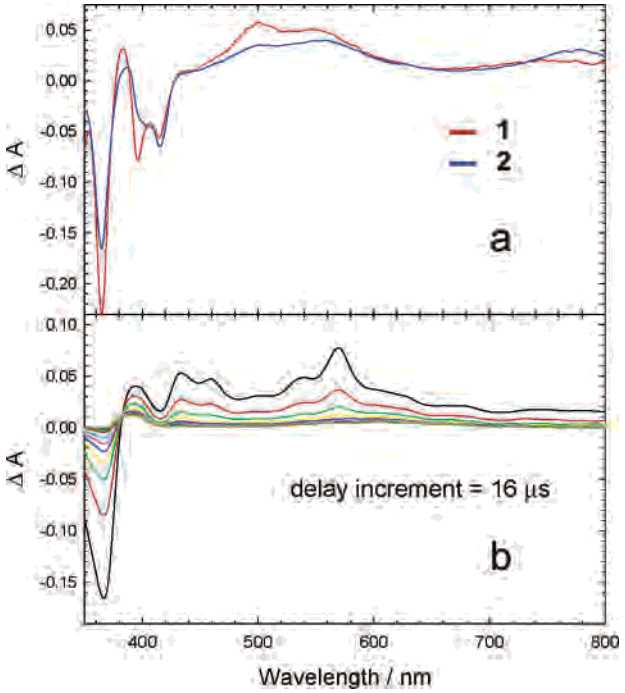

Figure 3. (a) Transient absorption spectra obtained for **1** (red) and **2** (blue) in degassed THF solution 1 μs delay following 355 nm excitation. (b) Transient absorption spectra obtained for **1** in the presence of MV^{2+} in degassed THF/CH_3CN (2:1) solution following 355 nm excitation. The black spectrum was obtained with 1 μs delay, and for succeeding spectra (in order of decreasing intensity) were obtained with 16 μs delay increments.

The geometry and energy of the lowest triplet excited state of HBC, **1**, and **3** were also computed with DFT. The results of the computations were very similar and indicate that the triplet excitation is localized in the HBC chromophore. This effect is clearly seen by comparing the computed bond lengths for the ground and triplet states of **1** (see Supporting Information). In particular, the bond lengths in the HBC chromophore in triplet **1** differ significantly from those for the ground state geometry; however, the bond lengths for the Pt−acetylide unit are virtually the same in the ground and first triplet state. The pattern of bond length differences between the lowest singlet and triplet states is very similar in HBC and **3**. Consistent with the notion of an HBC-localized triplet state, the calculated S_0-T_1 0−0 energy difference (energy gap between optimized geometry of the lowest triplet and singlet states) is very similar in the three compounds (last row, Table 2). Interestingly, the computed energy difference is remarkably close to the experimentally observed phosphorescence energy.

Transient Absorption Spectroscopy: HBC Triplet and Radical Cation Absorption. To provide additional information regarding the spectroscopy of the HBC triplet state and its reactivity in photoinduced electron transfer, nanosecond to microsecond time-resolved absorption experiments were carried out with Pt−HBCs **1** and **2** in THF solution ($c \approx 20$ μM). Figure 3a illustrates the time-resolved difference absorption spectra of **1** and **2** obtained at a series of delay times following 355 nm pulsed excitation. Both complexes

(44) Cooper, T. M.; Blaudeau, J. P.; Hall, B. C.; Rogers, J. E.; McLean, D. G.; Liu, Y. L.; Toscano, J. P. *Chem. Phys. Lett.* **2004**, *400*, 239−244.

exhibit bleaching (negative ΔA) in the region corresponding to the ground-state absorption ($\lambda < 420$ nm) combined with broad excited-state absorption bands extending throughout the visible into the near-IR region. These transients are attributed to the triplet excited state of the HBC chromophore. The transient absorption decay lifetimes for **1** and **2** in THF solution were 130 and 40 μs, consistent with the triplet assignment. Although the spectra of two complexes exhibit some subtle differences, they are generally very similar in band shape, which underscores the hypothesis that the triplet excitation is largely localized in the HBC chromophore.

Electrochemical studies were carried out on **1**−**3** (CH_2Cl_2 solution) in order to provide information concerning the potentials for oxidation and reduction of the HBC moiety. Unfortunately, well-resolved cyclic voltammetric waves were not observed for any of the materials, a result we attribute to aggregation and/or coating of the materials on the electrode surface. Nevertheless, a broad, quasi-reversible oxidation wave was observed for **1** at +0.8 V vs SCE. On the basis of this approximate potential combined with the triplet energy (2.14 eV), we estimate that the excited-state oxidation potential of the Pt−HBCs is $E_{1/2}(^3\text{Pt−HBC*/Pt−HBC}^{+\bullet}) \approx -1.3$ V vs SCE.[45] This indicates that the Pt−HBC triplet excited state is a strong reductant and photoinduced electron transfer to electron acceptors with reduction potentials more positive than −1.3 V will be thermodynamically favorable. In accord with this prediction, Stern−Volmer quenching studies using methyl viologen (MV^{2+}), which has a reduction potential of −0.40 vs SCE,[46] demonstrate that MV^{2+} quenches the triplet excited state of Pt−HBC **1** at the diffusion-controlled rate.

Transient absorption spectroscopy of a mixture of **1** (c = 4 μM) and MV^{2+} (c = 10 mM) in THF/CH_3CN (2:1 v/v) provides clear evidence that quenching involves photoinduced electron transfer to afford Pt−HBC radical cation ($\mathbf{1}^{+\bullet}$) and the reduced viologen ($MV^{+\bullet}$),

$$^3\mathbf{1}^* + MV^{2+} \rightarrow \mathbf{1}^{+\bullet} + MV^{+\bullet} \qquad (1)$$

As shown in Figure 3b, the transient absorption difference spectrum of the solution **1** and MV^{2+} is dominated by strong bleaching of the HBC ground-state absorption at ≈370 nm, combined with a strong absorption band at 570 nm, with a shoulder at 535 nm, along with another set of transitions in the 450−500 nm region. All of these bands are believed to arise from the Pt−HBC radical cation, $\mathbf{1}^{+\bullet}$. Although $MV^{+\bullet}$ exhibits absorption bands at 395 and 605 nm ($\epsilon \approx 3 \times 10^4$ and 1×10^4 M^{-1} cm^{-1}, respectively),[47] it is believed that these spectral features are obscured by the absorption of $\mathbf{1}^{+\bullet}$, which is considerably more intense. Given that $\mathbf{1}^{+\bullet}$ and $MV^{+\bullet}$ are produced in equimolar amounts in the transient absorption experiment and that the $\mathbf{1}^{+\bullet}$ absorption bands are much stronger compared to those of $MV^{+\bullet}$ allows us to estimate that the 570 nm absorption band of $\mathbf{1}^{+\bullet}$ has $\epsilon \geq 5 \times 10^4$ M^{-1} cm^{-1}.

(45) $E_{1/2}(^3\text{Pt−HBC*/Pt−HBC}^{+\bullet}) = E_{1/2}(\text{Pt−HBC/Pt−HBC}^{+\bullet}) - E_{\text{triplet}}$.
(46) Bard, A. J.; Faulkner, L. R. *Electrochemical Methods: Fundamentals and Applications*; Wiley: New York, 2000.
(47) Kosower, E. M.; Cotter, J. C. *J. Am. Chem. Soc.* **1964**, *86*, 5524−5527.

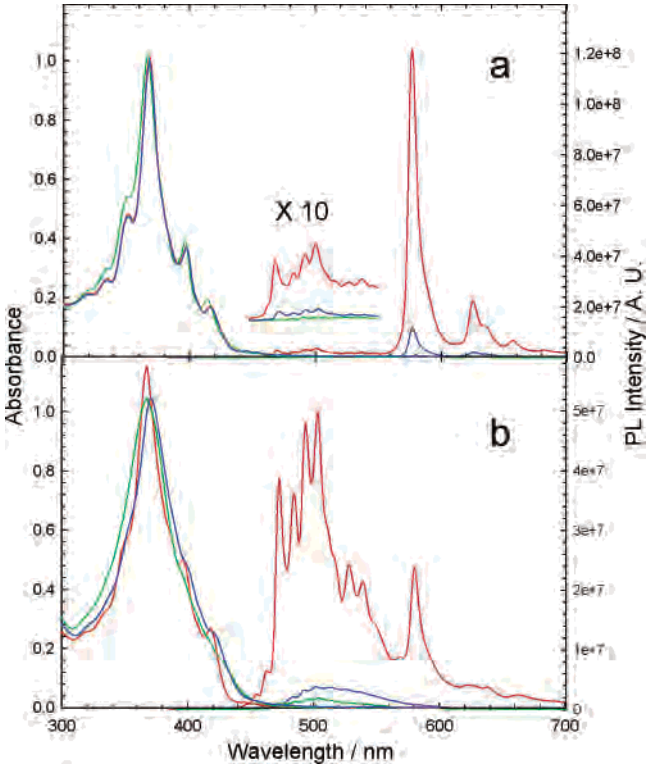

Figure 4. Absorption and photoluminescence spectra of (a) **1** and (b) **2** in THF (red), CH_2Cl_2 (blue), and hexane (green), $c \approx 5$ μM. Emission spectra were obtained on degassed solutions with matched absorbance at the excitation wavelength, and therefore, the intensities reflect the relative emission quantum yields.

Effects of Aggregation on the Triplet State. As noted in the Introduction, one of the principal aims of this investigation was to study the effect of aggregation on the triplet state of the HBC chromophore. To pursue this line of investigation, absorption, luminescence, and transient absorption spectra were obtained on the Pt−HBCs in a variety of solvents. A clear trend emerges from comparison of the data obtained in three solvents: THF, CH_2Cl_2, and hexane. With respect to solvation of the HBC chromophore, this series ranges from good (THF) to poor (hexane), and therefore, the degree of chromophore aggregation varies in the order hexane > CH_2Cl_2 > THF. In addition, as noted above, **2** has a stronger self-association constant, and consequently, the effects of aggregation are more pronounced for this complex in CH_2Cl_2 and hexane. Figure 4 compares the emission and absorption spectra of the two complexes in the three solvents ($c = 5 \times 10^{-6}$ M). Several trends are clear from the data. First, the absorption of the two complexes becomes slightly broader as the solvent is varied from THF to CH_2Cl_2 to hexane. This effect is most pronounced for complex **2**, where it is quite evident that the low-energy bands are very poorly defined in CH_2Cl_2 and hexane. The same effect is evident in the high-energy bands for complex **1**. We attribute the effects seen in hexane and to a lesser extent CH_2Cl_2 to the formation of aggregates, which are presumably formed by π-stacking of the HBC chromophores. Similar solvent effects on the absorption spectra of alkyl-substituted HBCs have been reported by Müllen and co-

workers under conditions where the chromophore is aggregated.[9,48]

More insight into the effects of aggregation on the photophysics comes from the photoluminescence data, which are also shown in Figure 4. First, it is quite evident that the intensity (quantum efficiency) of the emission (fluorescence and phosphorescence) decreases substantially along the series THF > CH_2Cl_2 > hexane. In particular, for **1**, the total emission yield decreases from 0.13 in THF to 0.028 in CH_2Cl_2. The quenching is even stronger in hexane, where the emission quantum yield is $\ll$0.01. A similar trend is seen for **2**, but in this case because the relative fluorescence yield is higher, it is also possible to discern that the vibronic structure that is present on the fluorescence band in THF is blurred in CH_2Cl_2 and hexane and the overall fluorescence appears more as a broad, red-shifted "excimer-like" band. While the phosphorescence of both complexes is strongly quenched by aggregation in CH_2Cl_2 and hexane, close inspection of the phosphorescence band shape of **1** reveals that it is almost the same in CH_2Cl_2 and THF, suggesting that the electronic structure of the triplet state is not strongly affected by aggregation. (Similar aggregation-induced quenching of the phosphorescence from **1** is observed in THF/hexane solvent mixtures as the proportion of hexane is increased, see Supporting Information for spectral data.)

The effect of aggregation on the triplet state of **1** and **2** was also probed by comparing the transient absorption spectra and triplet decay lifetimes of the two complexes in THF, CH_2Cl_2, and hexane. The spectra of the two complexes immediately following laser excitation are shown in Figure 5, and the transient absorption decay lifetimes are listed in Table 1. For each complex, the triplet decay lifetimes decrease in the sequence THF > CH_2Cl_2 > hexane; note that the triplet decays nearly 10-fold more rapidly in hexane compared to THF. These results clearly indicate that aggregation of the Pt−HBCs leads to quenching of the triplet state.

While there is a distinct effect of aggregation on the triplet lifetime, the effect of aggregation on the transient absorption difference spectra is less pronounced. For both complexes, the initial amplitude of the transient absorption is lower in CH_2Cl_2 and hexane compare to THF, which qualitatively indicates that the triplet yield is suppressed when the Pt−HBCs are aggregated. In addition, the position of the ground-state bleaching bands shifts slightly with solvent, consistent with the solvent effect on the absorption spectra. For complex **2**, the maximum of the visible triplet−triplet absorption band is slightly red-shifted in hexane compared to THF. By contrast, the visible region triplet−triplet absorption of complex **1** is almost unaffected by solvent.

Taken together, the spectral data suggest that aggregation has little effect on the electronic structure of the triplet state. Rather aggregation decreases the triplet yield and also accelerates triplet decay. The decrease in the triplet yield

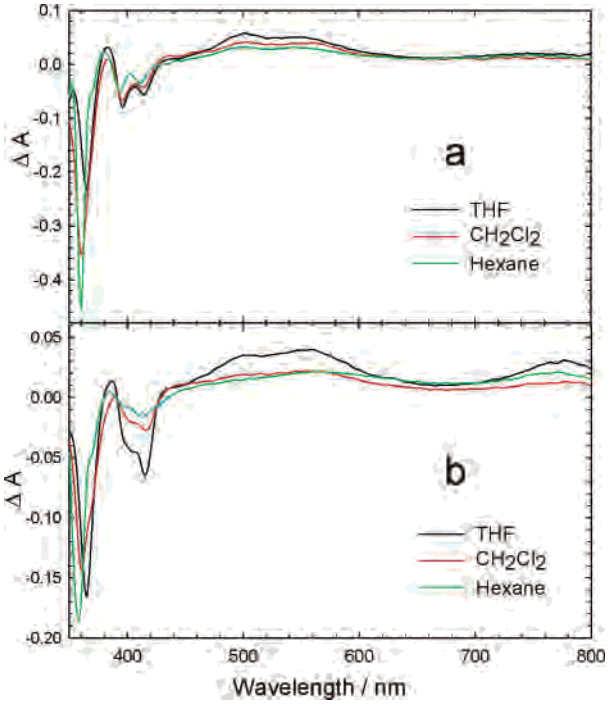

Figure 5. Transient absorption spectra obtained for (a) **1** and (b) **2** in degassed THF, CH_2Cl_2, and hexane solutions following 355 nm excitation. Spectra were obtained on degassed solutions with matched absorbance at 355 nm at the same laser power, and therefore, the relative intensities reflect the triplet yield.

concomitant with aggregation likely arises because the singlet excimer state is produced rapidly, and intersystem crossing in the excimer is less efficient than in the monomer singlet state. The lack of evidence for a strong aggregation effect on the phosphorescence or triplet−triplet absorption spectra suggests that a triplet excimer is not formed in the Pt−HBC aggregates (i.e., the triplet is localized on a single HBC chromophore unit, even in the aggregate). This finding is consistent with earlier work on triplet states in aromatic hydrocarbons which suggests that triplet excimers are not stabilized relative to the monomeric triplet states.[49−51]

While the available evidence indicates that the electronic structure of the HBC triplet in **1** and **2** is not strongly affected by aggregation, there is clear evidence that the lifetime of the triplet is reduced by aggregation. The origin of this effect is not clear; however, it likely arises due to the introduction of new low-frequency modes that increase the Franck−Condon factors for nonradiative decay of the triplet state. While triplet−triplet annihilation in the aggregates was considered as a possible pathway for the accelerated nonradiative decay, a study of the triplet lifetime as a function of laser power did not provide any evidence for the involvement of this pathway.

Summary and Conclusions

This report describes the synthesis and photophysical characterization of two HBCs that are functionalized with

(48) Wu, J. S.; Fechtenkotter, A.; Gauss, J.; Watson, M. D.; Kastler, M.; Fechtenkotter, C.; Wagner, M.; Müllen, K. *J. Am. Chem. Soc.* **2004**, *126*, 11311−11321.

(49) Lim, E. C. *Acc. Chem. Res.* **1987**, *20*, 8−17.

(50) Yanagidate, M.; Takayama, K.; Takeuchi, M.; Nishimura, J.; Shizuka, H. *J. Phys. Chem.* **1993**, *97*, 8881−8888.

(51) Yamaji, M.; Tsukada, H.; Nishimura, J.; Shizuka, H.; Tobita, S. *Chem. Phys. Lett.* **2002**, *357*, 137−142.

organometallic Pt−acetylide units. The ground-state absorption spectra of these novel Pt−HBCs are dominated by the bands characteristic of the HBC chromophore, with the exception of an additional, moderately intense band that appears at $\lambda \approx 417$ nm that is assigned to an allowed transition polarized along the axis of the π-conjugated Pt−acetylide unit. Photoluminescence and transient absorption spectroscopy reveal that the primary effect of the Pt−acetylide unit on the photophysics of the Pt−HBCs is to enhance the yield of the triplet excited state and promote its radiative decay (phosphorescence). Thus, both of the Pt−HBCs exhibit moderately efficient phosphorescence at room temperature at $\lambda_{max} \approx 578$ nm. The strong similarity of the phosphorescence of the two Pt−HBCs, combined with the results of triplet state DFT calculations, leads to the conclusion that the triplet is localized on the HBC chromophore. The phosphorescence affords the triplet energy of the HBC chromophore, $E_T \approx 2.14$ eV, and allows calculation of the S−T splitting, $\Delta E_{ST} \approx 0.6$ eV.

By analogy to other alkyl-chain-substituted HBCs, the Pt−HBCs have a strong tendency to aggregate, even in dilute solutions. Aggregation of the Pt−HBCs in dilute CH_2Cl_2 and hexane solutions is clearly evident from broadening of the ground-state absorption spectra and the appearance of broad, red-shifted excimer-like fluorescence. Interestingly, aggregation of the Pt−HBCs only leads to quenching of the triplet state, as evidenced by a substantial decrease in the phosphorescence intensity and the triplet lifetime. The results do not provide evidence for the existence of a triplet excimer, even when the ground state complexes are strongly aggregated in solution.

This investigation provides an excellent example of how the optical properties of the HBC chromophore can be strongly and favorably influenced by coupling to a transition metal unit. In the Pt−acetylide systems that are the subject of this investigation, the primary effect of the transition metal is to significantly enhance the probability of S_1-T_1 intersystem crossing and the rate of T_1-S_0 radiative decay. These properties could prove useful in optoelectronic device applications of metal-containing HBC systems. For example, it is now well-established that the use of phosphorescent chromophores can significantly enhance the quantum efficiency of light emission from organic light emitting diodes.[52,53] In addition, the efficiency of photoinduced charge separation in organic photovoltaic devices might be enhanced by the use of triplet excited-state chromophores as the active materials. These and other applications of Pt−acetylide-substituted HBCs are the subject of ongoing investigations.

Acknowledgment. We gratefully acknowledge the National Science Foundation (Grant No. CHE-0515066) and the Air Force Office of Scientific Research (Grant No. F49620-03-1-0127) for support of this work.

Supporting Information Available: Emission spectra of **1** for THF/hexane solvent mixtures; emission spectrum of **2** at 80 K; ^{1}H NMR spectra of **1**, **2, 3**, **6**, and **7**; ^{31}P NMR spectra of **1** and **2**; and frontier orbital density plots for HBC and **3** (11 figures). This material is available free of charge via the Internet at http://pubs.acs.org.

IC051788V

(52) Kwong, R. C.; Sibley, S.; Dubovoy, T.; Baldo, M.; Forrest, S. R.; Thompson, M. E. *Chem. Mater.* **1999**, *11*, 3709−3713.
(53) Baldo, M. A.; O'Brien, D. F.; You, Y.; Shoustikov, A.; Sibley, S.; Thompson, M. E.; Forrest, S. R. *Nature* **1998**, *395*, 151−154.